

PAPER • OPEN ACCESS

Speckle-based imaging (SBI) applications with spectral photon counting detectors at the newly established OPTIMATO (OPTimal IMAGING and TOMography) laboratory

To cite this article: Vittorio Di Trapani *et al* 2024 *JINST* **19** C01018

View the [article online](#) for updates and enhancements.

You may also like

- [Mapping the Conditions for Hydrodynamic Instability on Steady-State Accretion Models of Protoplanetary Disks](#)
Thomas Pfeil and Hubert Klahr
- [A 42 mV startup ring oscillator using gain-enhanced self-bias inverters for extremely low voltage energy harvesting](#)
Ryo Matsuzuka, Tatsuya Terada, Kaori Matsumoto et al.
- [Comparison of X-ray speckle-based imaging deflection retrieval algorithms for the optimization of radiation dose](#)
Helene Rouge-Labriet, Laurene Quenot, Sylvain Bohic et al.



PRIME
PACIFIC RIM MEETING
ON ELECTROCHEMICAL
AND SOLID STATE SCIENCE

HONOLULU, HI
Oct 6–11, 2024

Abstract submission deadline:
April 12, 2024

Learn more and submit!

Joint Meeting of
The Electrochemical Society
•
The Electrochemical Society of Japan
•
Korea Electrochemical Society

24TH INTERNATIONAL WORKSHOP ON RADIATION IMAGING DETECTORS
OSLO, NORWAY
25–29 JUNE 2023

Speckle-based imaging (SBI) applications with spectral photon counting detectors at the newly established OPTIMATO (OPTimal IMAGING and TOMography) laboratory

Vittorio Di Trapani,* Sara Savatović, Fabio De Marco, Ginevra Lautizi, Marco Margini and Pierre Thibault

*Department of Physics, University of Trieste, Via A. Valerio 2, Trieste, Italy
Elettra-Sincrotrone Trieste, Strada Statale 14, km 163.5, 34149 Basovizza, Italy*

E-mail: vittorio.ditrapani@units.it

ABSTRACT. Speckle-based imaging (SBI) is an advanced X-ray imaging technique that measures phase and dark-field signals, in addition to absorption signals. SBI uses random wavefront modulators to generate speckles and requires two images: one with a speckle pattern alone, and one with both the sample and speckles. SBI reconstruction algorithms retrieve three signals (transmission, refraction, and dark-field) by comparing the two images. In SBI, speckle visibility plays a crucial role in the retrieval of the three signals. When translating the technique from synchrotron sources to compact laboratory setups, the reduced coherence of the source and limitations in the available resolution yield lower speckle visibility, hampering the retrieval of phase and dark-field signals. In this context, direct-detection CdTe X-ray photon-counting detectors (XPCDs) provide an attractive solution, as they allow for a high detection efficiency and optimal spatial resolution enhancing speckle visibility. In this work, we present the newly established OPTIMATO (OPTimal IMAGING and TOMography) laboratory for X-ray imaging hosted at the Elettra synchrotron (Trieste, Italy). The setup for SBI with resolutions up to 15 μm including an XPCD and a charge-integrating flat-panel detector (FPD) has been used to acquire SBI data. The main limiting factors when moving SBI applications from synchrotron facilities to compact laboratory setups are summarized. The advantages of XPCDs over FPDs are discussed by comparing the SBI images obtained using both detectors. The potential of the spectral decomposition approach via multi-threshold acquisitions using XPCDs is briefly introduced. The results shown in this work represent the first step toward the realization of a multimodal and multiresolution X-ray facility.

*Corresponding author.

KEYWORDS: Computerized Tomography (CT) and Computed Radiography (CR); Multi-modality systems; Image reconstruction in medical imaging

2024 JINST 19 C01018

Contents

| | | |
|----------|--|----------|
| 1 | Introduction | 1 |
| 2 | Materials and methods | 2 |
| 2.1 | Experimental setup | 2 |
| 2.2 | Speckles visibility: from synchrotrons to laboratory sources | 3 |
| 3 | Results | 4 |
| 4 | Conclusions | 7 |

1 Introduction

Speckle-based imaging (SBI) is an X-ray phase-contrast imaging (XPCI) technique that enables the measurement of phase and dark-field signals, in addition to conventionally accessible absorption signals [1, 2]. SBI uses random wavefront modulators, such as sandpaper, to produce a reference speckle pattern at the detector plane. The technique requires the acquisition of two images: the first with the speckle pattern alone (reference image) and the second after introducing the sample into the beam (sample image). Compared with the reference image, the speckle pattern in the sample image is modulated in terms of intensity reduction (transmission signal), lateral displacement (refraction), and blurring (dark-field signal). SBI reconstruction algorithms operate by comparing the reference and sample images to retrieve the three signals. One key advantage of SBI over other XPCI techniques, such as grating-based imaging [3] and edge illumination (EI) [4], is that these use one or more grids usually produced via expensive lithographic methods to feature periodic apertures of a few microns, while SBI can use inexpensive random modulators such as sandpapers. Unlike grids, sandpaper does not require alignments or custom production processes, albeit at the cost of reduced visibility of the reference pattern.

As for other XPCI techniques, SBI has been first performed using coherent synchrotron sources. However, XPCI techniques can be adapted to laboratory facilities with quasi-coherent (micro-focus) sources, as reported in the literature [5–7]. To obtain optimal results in SBI, it is crucial to ensure the visibility of the speckles. Higher visibility is typically achieved with low-energy photons (<20 keV) and high statistics, such that the variations in speckle intensities dominate over the stochastic noise. However, these conditions are not always reproducible using compact X-ray sources. In this context, direct-detection CdTe X-ray photon-counting detectors (XPCDs) provide an attractive solution for SBI, featuring multiple advantages over the commonly employed indirect charge-integrating flat-panel detectors (FPD). First, thick (>0.5 mm) CdTe sensors allow for both high detection efficiency (up to 100 keV) and optimal spatial resolution. Second, the photon-counting readout counts each photon, regardless of its energy. This leads to better speckle visibility compared with an ideal charge-integrating detector that weights high-energy photons more than low-energy photons. Finally, by implementing one or more energy thresholds, XPCDs enable spectral imaging, thus providing information on the chemical composition of the samples under investigation.

This work presents the first SBI images at the newly established OPTIMATO (OPTimal IMAGING and TOMography) laboratory, an X-ray setup tailored for phase-sensitive techniques implemented in the framework of the Scattering-Based X-ray Imaging and Tomography (S-BaXIT) project hosted by the University of Trieste and Elettra synchrotron (Trieste, Italy). The X-ray setup is equipped with a high-brilliance microfocus liquid-metal-jet X-ray source, whereby images can be collected with both a spectral XPCD and a large-area FPD. Following a brief discussion on the primary challenges in adapting SBI technique from synchrotrons to compact laboratories, the main advantages of XPCDs over FPDs are demonstrated by comparing SBI images obtained using both detectors. Finally, the energy thresholds of the XPCD have been exploited to perform spectral imaging, highlighting how XPCDs can expand the range of applications available at the OPTIMATO laboratory.

2 Materials and methods

2.1 Experimental setup

The setup implemented at the OPTIMATO laboratory is shown in figure 1. In this setup, X-rays are generated by a microfocus, high-brilliance liquid-metal-jet source (MetalJet D2+, Excillum, Stockholm, Sweden), featuring a maximum acceleration voltage of 160 kV, maximum power of 250 W, and adjustable focal spot sizes ($\geq 15 \mu\text{m}$). The source can emit photons on two opposite sides, thereby allowing for the implementation of two semi-independent imaging branches. The experimental setup was assembled in a $7 \times 2.5 \text{ m}^2$ lead-shielded hutch. The first branch uses two optical tables ($2 \times 0.8 \text{ m}^2$ each), resulting in a maximum distance source-detector (SDD) of 4 m ('long branch'); the other uses a single table, allowing a maximum SDD of 2 m ('short branch'). The short branch, designed for high-resolution ($< 10 \mu\text{m}$) imaging, is currently under development.

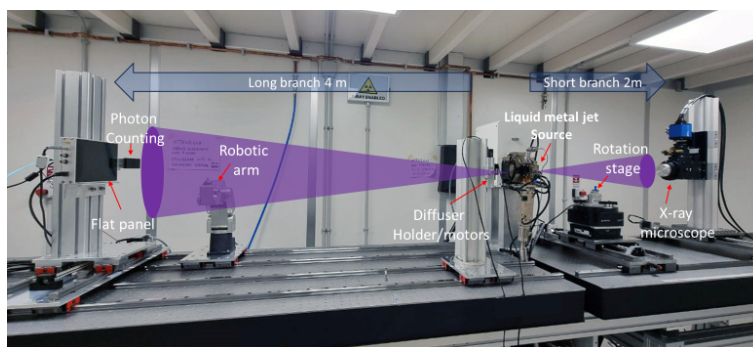


Figure 1. Picture of the X-ray setup implemented at the OPTIMATO laboratory.

The long branch, dedicated to SBI applications and micro-CT, is equipped with two detectors. The first is the LAMBDA 350k (X-Spectrum, Hamburg, Germany), an XPCD made of 3×2 Medipix3 chips bump-bonded with a single 1 mm thick CdTe sensor. This detector has an active area of $28 \times 42 \text{ mm}^2$, with a pixel pitch of $55 \mu\text{m}$. The Medipix3 chip implements two acquisition modes: single-pixel mode (SPM) and charge-summing mode (CSM). With SPM, each pixel works independently from its neighbors. Therefore, when the charge produced by a single photon spreads over multiple pixels, the photon can be detected by more than one pixel, potentially degrading the imaging performance of the detector [8]. The CSM overcomes the problem of charge sharing by summing the charges (from a

single photon) spread over a cluster of (2×2) pixels and assigning the count to the pixel receiving the highest fraction of the shared charge. In this mode, the energy of each event is correctly evaluated and the spatial accuracy is preserved [9]. This latter mode is best suited for applications requiring optimal spatial and spectral resolutions. The second detector available in the long branch is a FPD (CMOS 1512, Varex imaging, Salt Lake City, UT, U.S.A.) with a $200 \mu\text{m}$ thick micro columnar CsI scintillator, featuring an effective area of $145 \times 115 \text{ mm}^2$ and a pixel pitch of $74.8 \mu\text{m}$. In this branch, samples can be mounted on a Meca500 robotic arm (Mecademic Robotics, Montreal, Canada) with a repeatability of $5 \mu\text{m}$ and six degrees of freedom. The robotic arm can perform both translations and tomographic acquisitions, representing an ideal substitute for the assembly of linear and rotation stages, as commonly required by CT setups. Wavefront modulators such as sandpaper or gratings can be mounted onto two motorized translation stages (MFA-CC, MKS-Newport, Irvine, CA, U.S.A.) for horizontal and vertical motion. In this branch, the spatial resolution is limited by the source size.

2.2 Speckles visibility: from synchrotrons to laboratory sources

In SBI, the speckle pattern is generated by the interaction of an X-ray beam with a diffuser composed of random scatterers. The interaction of an X-ray beam with a diffuser composed of random scatterers generates speckles through two mechanisms: attenuation of incident radiation, and self-interference of wavefront through induced phase shifts. The visibility arising from propagation effects increases with the transverse and the temporal coherence in the diffuser plane. The transverse coherence increases for large source-diffuser distances and small source sizes, while the temporal coherence increases with the monochromaticity of the X-ray beam [10]. This explains why SBI is best suited for synchrotron facilities that provide long propagation distances, monochromatic radiation, and parallel-beam geometry while delivering high fluence rates.

When translating SBI from synchrotrons to laboratory sources, the visibility of speckles, which is a fundamental requirement for retrieving differential-phase and dark-field signals, is limited by several factors. In particular, the temporal coherence is limited by the polychromaticity of the X-ray beam, whereas the longitudinal coherence is limited by the finite source size and the reduced propagation distances achievable in a laboratory facility. Additionally, unlike in the case of synchrotron beamlines, where the propagation of the X-ray wavefront can be approximated by plane waves and the intensity of self-interferences in the speckle pattern increases with the actual distance diffuser-detector (z), in the cone beam geometry available with laboratory X-ray sources, propagation effects are described by spherical waves. In this case, the effective propagation distance (z_{eff}) required to produce the same effects obtained with a parallel beam is described by the Fresnel scaling theorem [11]:

$$z_{\text{eff}} = z/M \quad (2.1)$$

where $M = SDD/(SDD - z)$ is the geometrical magnification. Equation (2.1) shows that the cone-beam geometry requires larger z if compared to the case of parallel beam geometry. The effective propagation distances achievable at the OPTIMATO laboratory for a few fixed SDD are shown in figure 2. The plots show that for a fixed SDD, the maximum effective propagation distance is always obtained for $M = 2$. The maximum effective propagation distance attainable with the long branch is $z_{\text{eff}} = 1 \text{ m}$ with an actual distance diffuser/sample-detector $z = 2 \text{ m}$ and $SDD = 4 \text{ m}$.

Owing to the aforementioned limitations, the choice of the detection system plays a crucial role in the design of a compact setup for SBI. From the imaging point of view, the speckles feature a

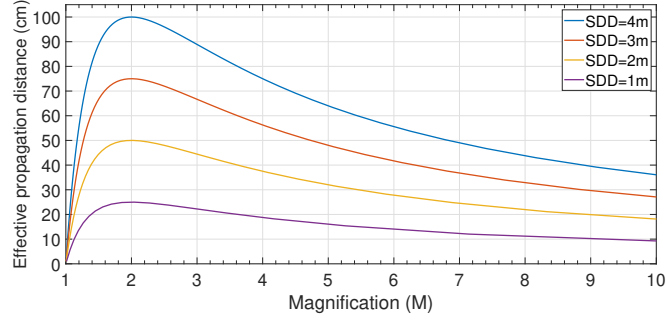


Figure 2. Plots of the effective propagation distance as a function of the magnification for different SDD settable in the long branch of the OPTIMATO laboratory.

noise-like pattern that must be resolved by the detection system and must be clearly distinguished from the stochastic noise. Considering these two factors, detectors featuring high spatial resolution and high detection efficiency are expected to improve speckle visibility. The spatial resolution is a property of the detection system which is generally described by the point spread function (PSF) [12], whereby a broad PSF blurs the speckles, reducing their visibility. In cone-beam X-ray setups where detectors have pixels larger than the source size, the PSF of the system PSF_{sys} depends both on the PSF of the detector PSF_{det} , the magnification (M) and source size (D) according to the following equation:

$$PSF_{\text{sys}} = \sqrt{\left(\frac{PSF_{\text{det}}}{M}\right)^2 + \left(\frac{M-1}{M}\right)^2 \cdot D^2} \quad (2.2)$$

Equation (2.2) shows that by increasing M it is possible to improve the spatial resolution up to the limits imposed by the source size ($PSF_{\text{sys}} \geq D$). However, for SBI, owing to the Fresnel scaling theorem (figure 2), speckle visibility is expected to decrease for $M > 2$. Therefore, the increase in spatial resolution and maximization of speckle visibility are competing factors. Consequently, when comparing different detectors for SBI applications, the highest speckle visibility is expected to be achieved by the one featuring an inherently higher spatial resolution (i.e., smaller PSF_{det}).

3 Results

This section shows the first SBI images obtained with the long branch at the OPTIMATO laboratory. The performances of the XPCD and the FPD are compared in terms of speckles visibility and SBI image quality. For all acquisitions, the source was used with a tube voltage of 50 kV, source size of $20 \mu\text{m}$, and emission power of 170 W. The XPCD has been used in charge-summing mode.

To better understand the potential of the XPCD compared to the FPD, the spatial resolution of both detectors has been evaluated. By using the slanted edge method [13], the full-width half maximum of the PSFs for the FPD and the XPCD were estimated to be $(130 \pm 3) \mu\text{m}$ and $(49 \pm 3) \mu\text{m}$, respectively. Figure 3 (a) displays the plots of the spatial resolutions attainable with both the XPCD and the FPD as a function of the magnification, according to eq. (2.2). The results show that the XPCD allows for better spatial resolution, especially for magnifications close to $M = 2$, where the effective propagation distance is maximized, enhancing propagation effects.

By setting a fixed $SDD = 150 \text{ cm}$, speckle visibility measurements have been performed with both detectors for different distances source-diffuser. As a diffuser, four layers of P120 sandpaper

with an average grit size of $125\ \mu\text{m}$ were employed. The visibility has been quantified as the standard deviation (σ) over the mean (μ) of the speckle pattern, i.e., $\text{visibility} = \sigma/\mu$. The measured speckle visibility as a function of the magnification is shown in figure 3 (b). The results show that the XPCD outperforms the flat panel, achieving higher visibility (up to a factor of 2) for all the magnifications. The results also show that, for both detectors, the maximum visibility is obtained for $M = 2$, for which the maximum z_{eff} is obtained, as shown in figure 2.

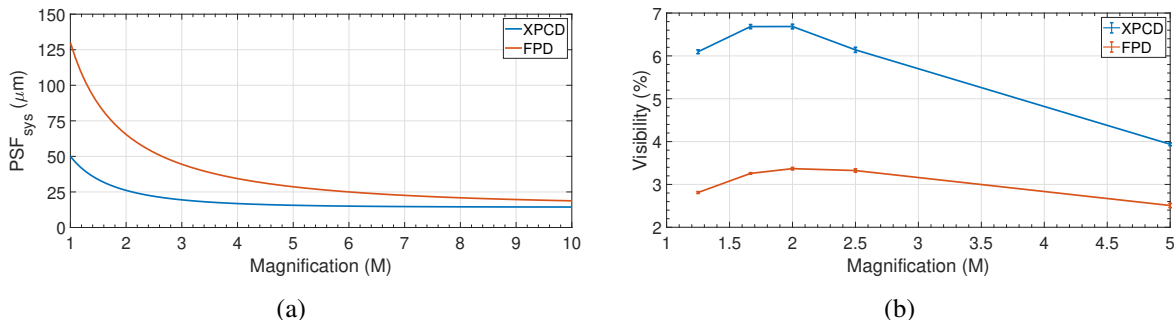


Figure 3. (a) PSF_{sys} as a function of the magnification for the XPCD and FPD available in the long branch, and a source size of $D = 20\ \mu\text{m}$; (b) visibility as a function of the magnification obtained with the FPD and the XPCD placed at 150 cm from the source.

To compare the performance of both detectors, two SBI scans have been performed with the optimal settings for speckle visibility as shown in figure 3(b), i.e., $SDD = 150\ \text{cm}$, distance source-diffuser 75 cm, and $M = 2$. The sample, composed of a water-filled pipette tip, a beetle glued to a pipette tip, and a wooden toothpick, was placed 80 cm from the source. From SBI datasets, transmission, dark-field, and refraction signals were reconstructed using the Unified Modulated Pattern Analysis (UMPA) software [14]. To increase the reliability of the results from UMPA, 20 diffuser positions were acquired. For the XPCD, dead pixels and artifacts arising from CdTe charge trapping effects, potentially affecting the speckle tracking algorithm, were processed using the filter presented in [15]. For each projection, multiple images were acquired and averaged to increase the photon statistics. With both detectors, the equivalent exposure time per projection was 60 s, ensuring a clearly distinguishable speckle pattern over the Poissonian noise. The transmission (T), dark-field (df), and horizontal differential-phase (dx) images reconstructed with UMPA for both SBI acquisitions are shown in figure 4. From a visual inspection of the dark-field and differential phase images in figure 4, it can be observed that for the XPCD, the sample features are clearly distinguishable from the background, whereas for the FPD, the noise partially or completely masks the details, thus leading to UMPA images of poorer quality. This is mainly due to the fact that, under the same experimental conditions, the XPCD allows for higher speckle visibility. In particular, the noise in FPD images (dx and df) occurs in regions where, owing to poor visibility, the fit of the UMPA model fails to converge, leading to the formation of bright/dark spots that affect the overall image quality. Referring to the dark-field signal, by inducing multiple scattering, the wood fibers in the toothpick are expected to produce a higher dark-field contrast when compared to the one generated by homogeneous features such as the water-filled pipette. As shown in the figure, this behavior is not correctly reproduced in the FPD image, where the water features stronger dark-field signals. The results also suggest that the visibility of approximately 3% achieved by the FPD is insufficient to allow SBI reconstructions

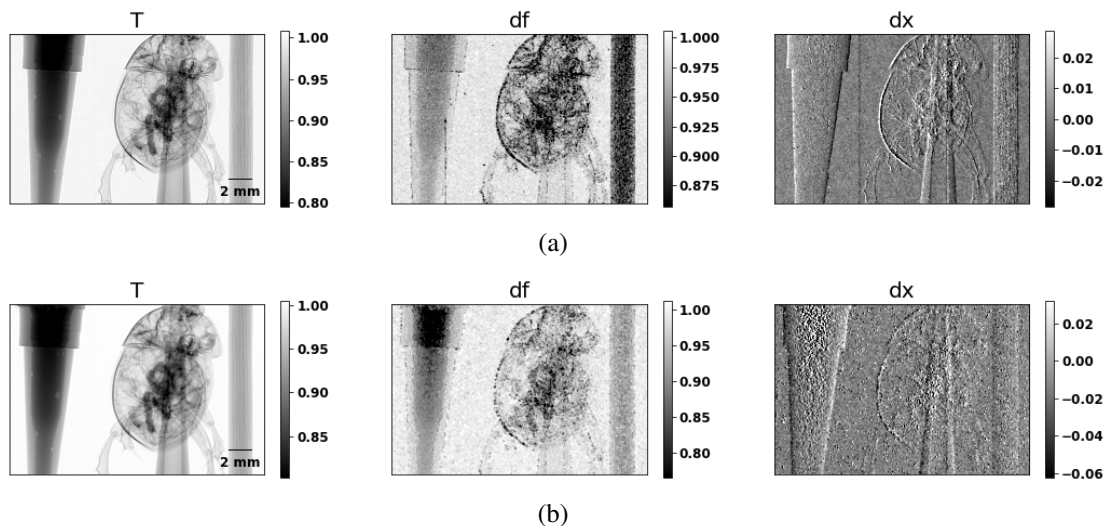


Figure 4. Transmission (T), dark-field (df), and horizontal differential-phase (dx) images reconstructed with UMPA from SBI datasets acquired with (a) XPCD, (b) FPD.

with UMPA. It is worth noting that if the FPD is not suitable for SBI with sandpaper, it cannot be excluded that custom diffusers made by more strongly absorbing materials would enable SBI with the FPD. Additionally, XPCI imaging with FPD and UMPA approach can be performed by using wavefront markers made by absorbing bar patterns that deliver high visibility [16]. It is also important to note that, by offering large detection areas, FPDs represent a valuable detection system for propagation-based imaging and conventional micro-CT of large samples.

The XPCD in the long branch also enables spectral imaging applications [17]. As an example, figure 5 shows a spectral decomposition with three materials for the same sample employed in the SBI scans. For the spectral acquisition, three conventional absorption images were acquired with three different energy thresholds ($thr_1 = 13$ keV, $thr_2 = 23$ keV, $thr_3 = 26$ keV), dividing the spectrum into three energy bins ([13–23] keV, [23–26] keV, and >26 keV) with the same amount of photons. The total exposure time per projection was 60 s. The material decomposition has been carried out using the minimum residual spectral decomposition algorithm presented in [18], setting three material bases: CaCO_3 (present in insect carapace), water, and carbon (present in wood and plastics). The results in figure 5(b), (c), and (d) show that the acquisition system is capable of distinguishing between water and plastic pipettes, as well as correctly identifying the carapace of the beetle. Combined with phase,

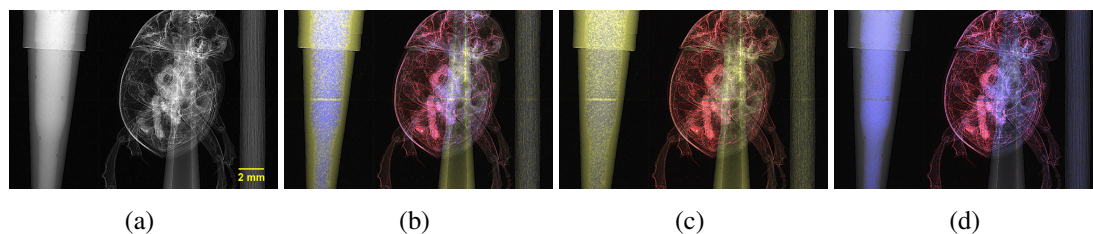


Figure 5. Absorption radiography (a). Overlay of (a) with decomposed bases: (b) CaCO_3 (red), water (blue), and carbon (yellow); (c) CaCO_3 and carbon; (d) CaCO_3 and water.

dark-field, and transmission signals, the spectral decomposition enhances the diagnostic capabilities of the proposed setup, thereby allowing for a more thorough analysis of the samples under examination.

4 Conclusions

In this work, we presented a newly established X-ray setup at the Elettra synchrotron (Trieste, Italy) implemented in the framework of the S-BaXIT project funded by the European Research Council. This setup is well-suited for a wide range of imaging applications, including absorption radiography and micro-CT, propagation-based imaging, various XPCI techniques such as SBI and speckle-based directional dark-field [19], and spectral imaging. The first SBI images taken with the long branch setup demonstrated that, under the same experimental conditions, XPCDs outperform the conventional FPD in terms of image quality for both differential-phase and dark-field images. In particular, by delivering higher speckle visibility, XPCDs prove to be an invaluable tool in the challenging task of translating SBI from synchrotrons to compact X-ray laboratories. Furthermore, the spectral capabilities of XPCDs expand the range of available applications.

The preliminary results shown in this work represent a starting point for the implementation of a reliable setup for SBI at the OPTIMATO laboratory. Several optimization studies for the choice of sandpaper, propagation distances, X-ray spectra, as well as the refinement of UMPA with the inclusion of spectral information to make the model more robust and reliable, are currently under investigation and will be the object of future works. The short branch of the setup is under development and will enable imaging applications with resolutions in the range $0.65 - 6.5 \mu\text{m}$. The two branches will provide a multimodal and multiresolution X-ray facility available to the community.

Acknowledgments

This work has received funding from the European Research Council (ERC) under the European Union's Horizon 2020 research and innovation program under Grant Agreement No. 866026.

Data and code availability. Data underlying the results presented in this paper may be obtained from the authors upon request. The Unified Modulated Pattern Analysis (UMPA) code is available at <https://github.com/optimato/UMPA>.

References

- [1] L. Quenot, S. Bohic and E. Brun, *X-ray Phase Contrast Imaging from Synchrotron to Conventional Sources: A Review of the Existing Techniques for Biological Applications*, *Appl. Sci.* **12** (2022) 9539.
- [2] S. Berujon, H. Wang and K. Sawhney, *X-ray multimodal imaging using a random-phase object*, *Phys. Rev. A* **86** (2012) 063813.
- [3] F. Pfeiffer et al., *Hard-X-ray dark-field imaging using a grating interferometer*, *Nat. Mater.* **7** (2008) 134.
- [4] A. Olivo, *Edge-illumination x-ray phase-contrast imaging*, *J. Condens. Matter Phys.* **33** (2021) 363002.
- [5] L. Brombal et al., *PEPI Lab: a flexible compact multi-modal setup for X-ray phase-contrast and spectral imaging*, *Sci. Rep.* **13** (2023) 4206.
- [6] I. Zanette et al., *Speckle-Based X-Ray Phase-Contrast and Dark-Field Imaging with a Laboratory Source*, *Phys. Rev. Lett.* **112** (2014) 253903.

- [7] J. Vila-Comamala et al., *High sensitivity X-ray phase contrast imaging by laboratory grating-based interferometry at high Talbot order geometry*, *Opt. Exp.* **29** (2021) 2049.
- [8] V. Di Trapani et al., *Characterization of the acquisition modes implemented in Pixirad-1/Pixie-III X-ray Detector: Effects of charge sharing correction on spectral resolution and image quality*, *Nucl. Instrum. Meth. A* **955** (2020) 163220.
- [9] R.M.N. Doesburg et al., *Spectrum measurement using Medipix3 in Charge Summing Mode*, *2012 JINST* **7** C11004.
- [10] J. Als-Nielsen and D. McMorrow, *Elements of Modern X-ray Physics*, Wiley (2011).
- [11] D. Paganin, *Coherent X-Ray Optics*, Oxford University Press (2006).
- [12] I.A. Cunningham, *Applied Linear-Systems Theory*, in *Handbook of Medical Imaging*, J. Beutel et al. eds., Vol. 1, SPIE Optical Engineering Press (2000), p. 79–160 [DOI:10.1117/3.832716.ch2].
- [13] E. Samei, M.J. Flynn and D.A. Reimann, *A method for measuring the presampled MTF of digital radiographic systems using an edge test device*, *Med. Phys.* **25** (1998) 102.
- [14] F. De Marco et al., *High-speed processing of X-ray wavefront marking data with the Unified Modulated Pattern Analysis (UMPA) model*, *Opt. Exp.* **31** (2022) 635.
- [15] V. Di Trapani and F. Brun, *Pre- and post-reconstruction digital image processing solutions for computed tomography with spectral photon counting detectors*, *Nucl. Instrum. Meth. A* **1010** (2021) 165510.
- [16] V. Di Trapani et al., *Unified Modulation Pattern Analysis (UMPA) algorithm for 1D sensitive X-ray phase contrast imaging techniques*, *2023 JINST* **18** C01059.
- [17] R. Ballabriga et al., *Photon counting detectors for x-ray imaging with emphasis on CT*, *IEEE Trans. Radiat. Plasma Med. Sci.* **5** (2021) 422.
- [18] V. Di Trapani, L. Brombal and F. Brun, *Multi-material spectral photon-counting micro-CT with minimum residual decomposition and self-supervised deep denoising*, *Opt. Exp.* **30** (2022) 42995.
- [19] R. Smith et al., *X-ray directional dark-field imaging using Unified Modulated Pattern Analysis*, *PLOS One* **17** (2022) e0273315.